Structural motifs of pre-nucleation clusters

Y. Zhang, I. R. Türkmen, B. Wassermann, A. Erko, and E. Rühl

Citation: The Journal of Chemical Physics **139**, 134506 (2013); doi: 10.1063/1.4823497

View online: http://dx.doi.org/10.1063/1.4823497

View Table of Contents: http://scitation.aip.org/content/aip/journal/jcp/139/13?ver=pdfcov

Published by the AIP Publishing

Structural motifs of pre-nucleation clusters

Y. Zhang,[1] I. R. Türkmen,[1] B. Wassermann,[1] A. Erko,[2] and E. Rühl[1]
[1]*Physikalische Chemie, Freie Universität Berlin, Takustr. 3, 14195 Berlin, Germany*
[2]*Helmholtz-Zentrum Berlin, Albert-Einstein-Str. 15, 12489 Berlin, Germany*

(Received 6 July 2013; accepted 12 September 2013; published online 4 October 2013)

Structural motifs of pre-nucleation clusters prepared in single, optically levitated supersaturated aqueous aerosol microparticles containing $CaBr_2$ as a model system are reported. Cluster formation is identified by means of X-ray absorption in the Br K-edge regime. The salt concentration beyond the saturation point is varied by controlling the humidity in the ambient atmosphere surrounding the 15–30 μm microdroplets. This leads to the formation of metastable supersaturated liquid particles. Distinct spectral shifts in near-edge spectra as a function of salt concentration are observed, in which the energy position of the Br K-edge is red-shifted by up to 7.1 ± 0.4 eV if the dilute solution is compared to the solid. The K-edge positions of supersaturated solutions are found between these limits. The changes in electronic structure are rationalized in terms of the formation of pre-nucleation clusters. This assumption is verified by spectral simulations using first-principle density functional theory and molecular dynamics calculations, in which structural motifs are considered, explaining the experimental results. These consist of solvated $CaBr_2$ moieties, rather than building blocks forming calcium bromide hexahydrates, the crystal system that is formed by drying aqueous $CaBr_2$ solutions. © *2013 AIP Publishing LLC*. [http://dx.doi.org/10.1063/1.4823497]

I. INTRODUCTION

Nucleation processes have been studied for a long time, since these are of fundamental interest to crystal formation as well as of importance to environmental science, materials research, and life sciences.[1–4] Especially in the atmospheric environment, metastable states of supercooled or supersaturated aerosol species are known to play a central role, e.g., for the formation of precipitation and reactive processes.[5] Various nucleation models have been considered in the past. Classical nucleation theory initiated by Volmer and Weber and subsequent improvements require the formation of critical nuclei by stochastic density fluctuations in the supersaturation regime in order to overcome the barrier for spontaneous growth.[6,7] In aqueous electrolyte solutions this implies that desolvation of the ions must occur via a cluster phase.[8] Such phenomena have been investigated by Myerson and co-workers by measuring diffusion coefficients in supersaturated solutions, which leads to an estimate of the critical cluster size.[9]

More recently, evidence for stable pre-nucleation clusters has been found, which were studied by isothermal titration calorimetry.[10,11] It was stated that the structures of these clusters probably do not relate to the macroscopic bulk. In addition, a variety of different *in situ* approaches have been used in the past to study the crystal formation process.[12]

Initialization of cluster formation from aqueous solutions starts with increasing solute concentration by desolvation of the fully solvated ions leading to ion-pair formation or Bjerrum pairs. The occurrence of these species has been subject of discussion.[13] Earlier work indicated that associates of these species contribute to cluster formation.[9] Recent studies from modeling provide information on the structure of pre-nucleation clusters.[14] However, detailed experimental *in situ* studies on such species are missing to date. This provides the motivation for the present work, in which we aim to prepare the initial species contributing to pre-nucleation cluster formation in single, supersaturated aqueous droplets and probe these by tunable X-rays. Hygroscopic properties of individual deposited sub-micron-sized particles were studied recently by X-ray microscopy leading to distinct spectral changes and shifts as a function of humidity, where also phase transitions were investigated.[15] Single microparticles are on the other hand most often electrodynamically trapped for reaching the supersaturation regime, in which they are kept in an equilibrium with their surroundings.[8,9,16–20] The charge-to-mass ratio is a crucial quantity for stable trapping of single particles. This quantity may significantly change during the experiments, if ionizing radiation, such as X-rays, are used for probing the electronic structure of single trapped particles.[21] This requires to adjust properly the stabilizing ac-frequency in order to localize the particles in the electrodynamic trap. It is also known that highly charged liquid droplets lead to instabilities in particle position, especially near the Rayleigh limit, where mostly electrical charges but only small amounts of the liquid get lost via the formation of Rayleigh jets.[22] An alternative approach for trapping single microdroplets is optical levitation,[23,24] especially since this is independent of the charge state of the droplets and appears to be the most suitable trapping technique for probing the electronic structure of single microparticles.

Aqueous $CaBr_2$ solutions are used as a model system, for which structural information of the solvated ions and pre-nucleation clusters is obtained from near-edge spectroscopy, an element-selective probe of the local electronic structure, which is tightly related to the geometric structure near the absorbing site. Calcium bromide is known to crystallize at room temperature in the dry crystal in a distorted orthorhombic

lattice (Pnnm).[25] Furthermore, calcium bromide is known to be highly hygroscopic, so that hexahydrates of calcium bromide ($CaBr_2 \cdot 6\ H_2O$) are formed from aqueous solution.[26] These crystallize in the space group P321.[27] There, the calcium is surrounded by nine water molecules. Similar findings have been reported for solvated calcium ions in combination with molecular dynamics calculations, from which a water coordination number of eight was deduced.[28] Concentrated calcium chloride solutions have been studied by EXAFS and near-edge spectroscopy providing evidence for solvent-bridged ions pairs.[29] The experimental results reported in this work go a step further, since single levitated droplets can reach significantly higher solute concentration far beyond the saturation point than can be reached in liquid cells.[30] The experimental results gathered at the Br K-edge are compared to results from model calculations in order to derive detailed information on structural changes occurring upon the transition from dilute solutions to the crystalline solid via supersaturated solution. Possible structural motifs of pre-nucleation clusters are determined, which are formed by ionic solutes in highly concentrated, supersaturated solutions.

II. EXPERIMENTAL

The experimental setup consists of a levitation cell, in which a single aqueous microdroplet is exposed to a beam of monochromatic synchrotron radiation from the KMC-2 beamline at the storage ring BESSY II (Helmholtz Center Berlin, Germany). A schematic diagram of the setup is shown in Figure 1. This beamline delivers up to 10^{10} photons/s at a focal spot size of 300 (horizontal) μm × 900 (vertical) μm. Further focusing of the radiation is accomplished by a polycapillary lens down to 25 μm × 25 μm spot size, so that the interaction with the optically levitated aqueous microdroplets is substantially improved.[31] Detection of X-ray fluorescence which is emitted from the levitated microparticles exposed to monochromatic X-rays is measured by a Si-PIN photodiode (Silicon Sensor, PR 200-7-CER-2 PIN). Near-edge spectra are measured by energy scans at the Br K-edge as a function of solute concentration, which is varied by adjusting the humidity in the levitation cell.

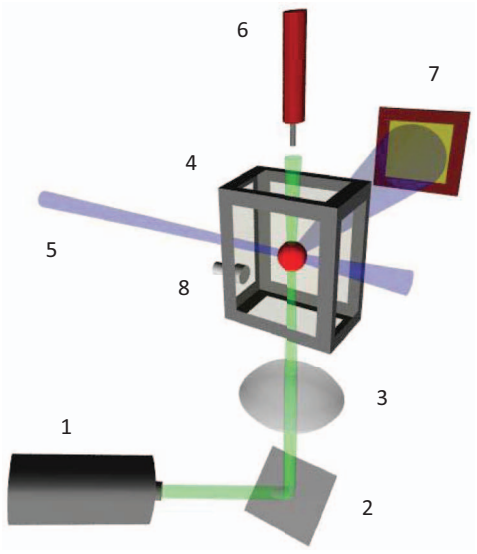

FIG. 1. Schematic presentation of the experimental setup. 1: Levitation laser, 2: mirror, 3: lens, 4: levitation cell, 5: synchrotron radiation, 6: piezo injector, 7: fluorescence detector, 8: humidity sensor.

TABLE I. Relative humidity (RH), corresponding molalities (m), and saturation ratios (S) of single, levitated, aqueous $CaBr_2$ solution microdroplets. Experimental energy shifts of the Br K-edge (ΔE_{edge}) relative to the Br K-edge position of the dilute solution (E = 13 468.5 ± 0.3 eV) are reported. Furthermore, the shift of the white line position (ΔE_{WL}) relative to that of the dilute solution (E = 13 475.0 ± 0.3 eV) is shown (cf. Figure 2).

RH (%)	m (mol/kg)	S	ΔE_{edge} (eV) ± 0.4 eV	ΔE_{WL} (eV) ± 0.4 eV
Dilute solution	2.72	0.38	0.0	0.0
63.3	7.17	1.00	− 2.4	− 1.8
61.7	8.32	1.16	− 4.1	− 3.3
58.3	10.40	1.45	− 4.3	− 2.8
45.1	14.34	2.00	− 4.7	− 3.3
Solid	...	...	− 7.1	− 7.5

The calibration of the photon energy scale is performed using the K-edges of molecular bromine (cf. Ref. 32) and a zinc foil by employing a Si (111) crystal monochromator. This procedure allows us to reach a wavelength resolution of $\lambda/\Delta\lambda \approx 5000$. The precision of the near-edge measurement is of the order of 0.25 eV at the Br K-edge (13.465 keV), as verified by repeated near-edge spectra of the same droplet. As a result, we use error limits of ±0.3 eV, which apply to the energy positions of the K-edge and white line of dilute and highly concentrated $CaBr_2$ solution droplets (see Table I). This appears to be justified, since the determination of the edge positions can be determined with a precision well below the energy resolution of the beam line (cf. Ref. 33).

Microdroplets are produced by a home-made piezo nozzle with a diameter of ∼50 μm. These shrink in size after the loss of water during levitation to the diameter regime of typically 15–30 μm. The nozzle is placed on top of the levitation cell, so that single microdroplets get conveniently trapped by a cw-laser beam (Coherent, Verdi, $\lambda = 532$ nm, ≈1 W power). The laser beam is focused by a lens (f = 80 mm) to a point, which is close to the crossing with the monochromatic synchrotron radiation (cf. Figure 1).

The position of the levitated particle relative to the X-rays is monitored by an optical microscope. The temperature and relative humidity are controlled by a combined temperature and humidity sensor SHT75 (Sensirion, Eval. Kit EK-H2). It is mounted in the wall of the optical levitation chamber in order to measure the ambient conditions close to the levitated microdroplets. The relative humidity is adjusted by using a mixture of dry and wet nitrogen, which is passed through two Nafion moisture exchanger tubes (Perma Pure, METM-Series). This allows us to investigate single, supersaturated microparticles in a thermodynamic equilibrium with their atmospheric surroundings.

The anhydrous $CaBr_2$ is of commercial quality (Alfa Aesar, Karlsruhe, Germany, purity 99.5%). Distilled water is used as a solvent after further purification by a 0.2 μm filter.

The molality of the supersaturated $CaBr_2$ solution at a given relative humidity is calculated from the temporal change in droplet radius, which is driven by diffusion-limited evaporation (cf. Ref. 34). The solute concentration of the supersaturated solutions is estimated from the formula of diffusion limited evaporation used before:[35]

$$a^2 = a_0{}^2 + S_{ij}(t - t_0), \quad (1)$$

where a_0 is the initial radius of the droplet at the time t_0, which is derived from Mie scattering and a is the radius at the time t. S_{ij} depends on the bimolecular diffusivity, molecular weight of the solvent, temperature, and the density of the aqueous solution. The solute concentration is also shown in Table I. The state of matter and size of the levitated droplets is constantly monitored during the experiments by angle-resolved Mie scattering. The analysis of the scattered light of the levitation laser is performed similar to our previous work.[17–19]

III. MODEL SIMULATIONS

Model simulations are performed at the Conrad-Zuse-Computing Center (Berlin/Hannover, Germany). The experimental results are simulated by model calculations as follows: Solvated species formed from calcium bromide are modeled in their equilibrium configuration by molecular dynamics (MD) calculations using the program package CP2K.[36] Point charges on the ions, $q_{Ca} = 2.40\ e$ and $q_{Br} = -1.20\ e$, are taken from FDMNES-SCF calculations[37] in order to simulate electrolytic dissociation in aqueous solutions. Note that for the dilute solution a slightly changed value of $q_{Br} = -1.30\ e$ is used in order to fully reproduce the experimental results for solvated Br^- in the case of the dilute solution. The charges on water, $q_O = -0.82\ e$, $q_H = 0.41\ e$, and the Lennard-Jones potential parameters are taken from the previous MD-simulations on the same system.[38] Equilibrium is reached after 2.5 ps of simulation time by using the conventional Nóse cryostat procedure. A periodic simulation cell of 15 Å ×15 Å ×15 Å containing on the average 150 H_2O molecules and up to 66 ions is adjusted to reproduce the saturation conditions occurring in the experiments. The number of anions and cations is selected in order to fulfill electroneutrality conditions in the simulation cell.

Core-level spectra at the Br K-edge involving solvated anions or pre-nucleation clusters are simulated by using the software package FDMNES (finite difference method for near edge spectroscopy).[37] This program allows for fully relativistic monoelectronic density functional theory calculations (DFT-LSDA). Earlier work made use of the FEFF8-code for simulating K-edges.[39] Their approach was adopted, whereby best agreement with the experimental results was achieved by using the SCF option of FDMNES. The potential is calculated at each cycle, where the calculations reach self-consistency and the final XANES simulation use this SCF potential. Note that no improvement of the simulations was achieved by using the well-known "Z + 1" approximation.[40] Finally, the calculated spectra are convoluted by Lorentzian line shapes and an arctan-based energy-dependent broadening formula:[41]

$$\Gamma = \Gamma_{\text{Hole}} + \Gamma_{\text{m}} \left(\frac{1}{2} + \frac{1}{\pi} \arctan \left\{ \frac{r_m}{E_{l\,\text{arg}}} \left(e - \frac{1}{e^2} \right) \right\} \right). \quad (2)$$

Here, $e = (E - E_F) / E_{cent}$; Γ_{Hole} is the core level width which is varied slightly above 1 eV for yielding best agreement with the experimental results. Γ_m, E_{cent}, and E_{larg} correspond to the maximum width of the final state, the central energy, and the width of an arctangent function, respectively. The typical values used in this work for these quantities are 15 eV, 3 eV, and 30 eV, respectively. In order to check for any erroneous shifts in the calculated near-edge spectra, which might be connected to changes in total number of ions or molecules in the computational cell, additional ions and solvent molecules are added at positions far away from the core excited bromine species. However, neither changes in spectral shape nor K-edge position were deduced from these additional calculations.

IV. RESULTS AND DISCUSSION

Figure 2 shows the experimental results of variable concentration $CaBr_2$ solution droplets. The absolute energy scale of these spectra is determined after proper calibration of the X-ray monochromator at the Br K-edge (see Sec. II) using the dilute $CaBr_2$-solution as a reference for the subsequent studies on single levitated microdroplets. The dilute solution well below the saturation point (2.7 molal (S = 0.38)) has been recorded by using two polymer tape slides in order to avoid evaporation during the experiments (cf. bottom spectrum in Figure 2). This solute concentration is well below the saturation point, which is reached at a 7.17 molal solution or at 63.3% relative humidity (S = 1). In addition, solid $CaBr_2$ is also investigated under the same conditions in order to have another reference point for probing

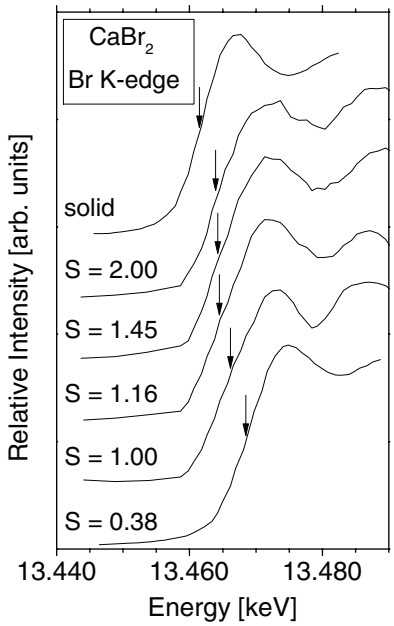

FIG. 2. Experimental near-edge spectra of supersaturated calcium bromide microdroplets at the Br K-edge as a function of saturation ratio S. For a comparison the near-edge spectrum of the dilute solution (S = 0.38, bottom) and the anhydrous solid (top) are shown. The arrows correspond to the edge positions (cf. Table I and text for further details).

energy shifts of the near-edge features occurring in single levitated microparticles (cf. top spectrum in Figure 2). In dilute solutions it is assumed that the bromine anions are fully solvated by water,[29] whereas the dry solid is dominated by an distorted orthorhombic structure at ambient conditions.[25] The near-edge spectra of both samples are significantly shifted in energy, whereas the spectral shape appears to be quite similar. Specifically, the absorption of the solid is red-shifted by 7.1 ± 0.4 eV relative to the dilute solution (cf. Table I). This spectral shift is determined by the change in energy position of the Br K-edge position, which is derived from the first derivative of the experimental yield spectra (E_{exp}), corresponding the inflection point at the edge jump. Alternatively, the spectral shift in "white line" position, the broad spectral maximum above the edge-jump,[42] is determined for both samples, yielding 7.5 ± 0.4 eV (cf. Table I). A slightly larger shift of 7.9 ± 0.4 eV is deduced from the "black line" position, the minimum in intensity above the "white line."[43] This indicates that the spectral shape at the Br K-edge is not changing significantly upon solvation of bromine anions in aqueous solution, rather than the excitation energy, as can be seen from Figure 2. The near-edge spectra of the saturated solution (S = 1) and supersaturated solutions (S > 1) are indeed observed between these bracketing conditions (cf. Figure 2).

Figure 2 also shows near-edge spectra of four different saturation ratios S, reaching from the saturated solution (S = 1) to S = 2, corresponding to a molality ranging between 7.17 and 14.34. The energy position of the K-edge is shifted to lower energy, corresponding to a spectral red-shift, as a function of solute concentration, as compared to the dilute solution (bottom spectrum in Figure 2). This red-shift ΔE increases as a function of supersaturation, as observed for the Br K-edge position (ΔE_{edge}) and the energy position of the white line (ΔE_{WL}, cf. Table I). The shape of the near-edge spectra remains fairly similar, implying that only slight changes in electronic structure occur as a function of supersaturation. Clear changes in near-edge structure are evidently not visible from these results, indicating that gradually the chemical environment is changed near the absorbing bromine sites, i.e., there is evidence for cluster formation in highly concentrated solution droplets in the supersaturation regime. Considering earlier work,[8,9] it is straightforward to assume that either desolvation of the anions and cations may take place, whereby their local aqueous surroundings are replaced by oppositely charged ions, as a result of electrostatic interactions between the solvated ions. This might be expected to lead initially from solvated Br^- via solvated $CaBr_2$ monomers to larger solvated cluster structures, corresponding to pre-nucleation clusters. This would imply that desolvated crystalline species represent plausible structures of pre-nucleation clusters, which are growing in size as S is increased. These are below the critical size permitting spontaneous and fast growth and the phase transition into a crystalline solid, since no phase transition to solid particles is observed by elastic light scattering under the present conditions. Evidently, there are size effects in cluster formation and possible ion desolvation in solution, which are observed by an energy shift of the K-edge position as well as the white line position at the Br K-edge. On the other hand, as an alternative plausible structural motif, water might surround the Ca^{2+} sites and solvent-shared ion aggregates might be formed with increasing concentration.[29,30] The latter structural motif appears to be intuitively more plausible, because crystalline hydrates are known to be formed from aqueous solution.[26] Therefore, from this point of view pre-nucleation clusters would likely contain water, rather than clusters of anhydrous $CaBr_2$. This aspect will be discussed along with model calculations below.

We also note that there are in the Br K-continuum oscillations in the cross section of all solute concentration, which are most likely due to the lowest energy part of the EXAFS signal. In general, one would expect that such EXAFS oscillations would increase in amplitude as the number density of counter ions containing heavy atoms increases, which would indicate strong scattering from the nearest neighbor shell in $CaBr_2$-clusters. This contribution is expected to be more intense from the heavy atoms than from the solvent. In addition, the distance between the shell of counter ions is expected to be larger upon ion pairing and cluster formation compared to ion hydration, which would correspond to a higher frequency of the oscillatory part of the signal in the Br K-continuum than one would expect from the solvent in a dilute solution. This explains qualitatively that there are oscillations in the cross section at all solute concentrations. However, data permitting even a preliminary EXAFS analysis as well as a detailed analysis of the continuum signal shown in Figure 2 goes beyond the scope of the present work.

Deeper insights into plausible structures that are formed upon evaporation of water from trapped, supersaturated microparticles are obtained from model calculations, as shown in Figure 3. The following structural motifs occurring in supersaturated solutions are considered: (i) solvated ions; (ii) solvated pairs, (iii) clusters of variable size containing no water, as well as (iv) solvated structures forming stable aggregates. It is aimed to derive from these model structures characteristic sites, which explain the spectral shifts by using a building block approach. This is accomplished by calculating for each model structure a near-edge spectrum, as shown in Figure 4. Specifically, we have considered the following structures for simulating the experimental results:

(i) Solvated Br^- (cf. Figures 3(a) and 4(a)), serves as a reference for deriving the spectral shifts in supersaturated solutions.
(ii) Solvated $CaBr_2$, corresponding to a solvated monomer, provides only corner sites C in solute clusters (cf. Figures 3(b) and 4(b)). The Ca^{2+}–Br^- distance is close to 3.0 Å after equilibration in the aqueous environment. Note that the linear isomer is found to be not stable. The spectral shift of the edge position relative to the calculated spectrum of the fully solvated Br^- is −3.2 eV.
(iii) Solvated calcium bromide dimers $(CaBr_2)_2$, where a corner site is marked by C and a two-fold coordinated edge site denoted by E is contained (cf. Figures 3(c), 4(c), and 4(g)). The spectral K-edge shift of the corner sites (C) relative to the solvated Br^- is −4.0 eV, which is similar in magnitude as the results compiled

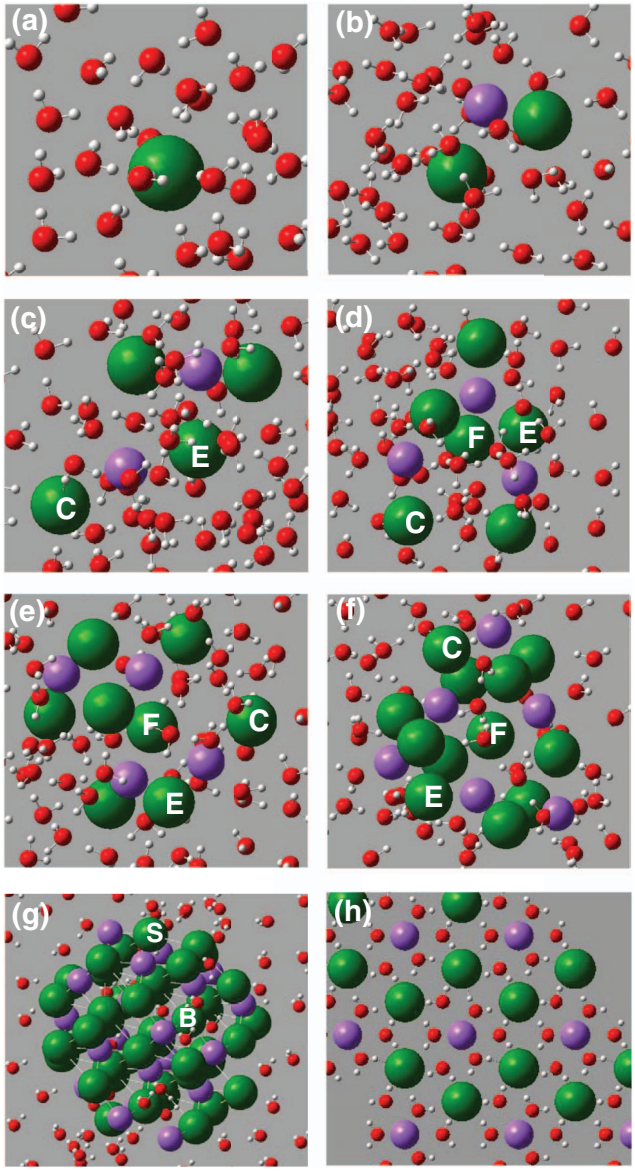

FIG. 3. Calculated structural motifs of solvated $CaBr_2$-clusters: (a) solvated Br^-; (b) solvated monomer $CaBr_2$; (c) solvated dimer $(CaBr_2)_2$; (d) solvated trimer $(CaBr_2)_3$; (e) solvated tetramer $(CaBr_2)_4$; (f) solvated hexamer $(CaBr_2)_6$; (g) solvated $(CaBr_2)_{22}$; (h) $CaBr_2 \cdot 6\ H_2O$ crystal. C: corner site, E: edge-site, F: face site, B: bulk site; S – surface site (see text for further details).

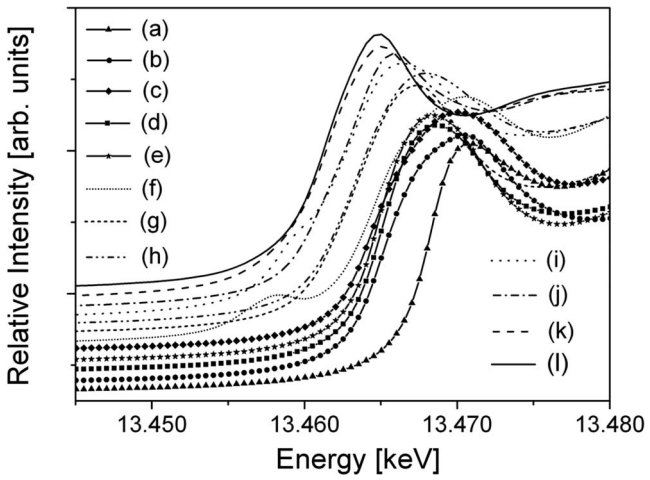

FIG. 4. Calculated near-edge structures of the structural motifs shown in Figure 3: (a) solvated Br^-; (b) solvated monomer $CaBr_2$; (c) solvated dimer: corner site; (d) solvated trimer: corner site; (e) solvated tetramer: corner site; (f) $CaBr_2 \cdot 6\ H_2O$ crystal; (g) solvated dimer: edge site; (h) solvated trimer: edge site; (i) solvated tetramer: edge site; (j) solvated tetramer: face site; (k) $(CaBr_2)_{22}$: surface site; (l) anhydrous crystal of $CaBr_2$: bulk site. Distinct shoulders in the pre-edge regime are due to hydrogen bonding with the surrounding water (the spectra are vertically slightly displaced, see text for further details).

in Table I. There are slightly different absorption energies, which are due to the solvation structure near this site, accounting for a calculated energy difference of 0.5 eV. Furthermore, for the twofold coordinated edge-sites (E) one derives a red-shift of 4.7 eV relative to the solvated Br^-.

(iv) Trimers $(CaBr_2)_3$ yield a three-dimensional structure retaining the symmetry of the crystal (see Figures 3(d), 4(d), and 4(h)). This provides no additional change in simulated spectral shape compared to the dimer (cf. Figure 4(c)). Only the number of edge- and corner-sites is increased in the trimer as compared to the dimer. Note that for CaF_2 a circular isomer was identified,[2] which is not stable in the case of solvated $CaBr_2$.

(v) Solvated calcium bromide tetramers $(CaBr_2)_4$ provide corner (C), edge (E), and face sites (F) (cf. Figures 3(e), 4(e), 4(i), and 4(j)). The face sites give rise to a red-shift in K-edge energy of 6.8 eV relative to the solvated Br^-, whereas the corner sites yield similar values as calculated for the Bjerrum pair and the dimer or trimer. Note that the isomers, which were identified for CaF_2,[2] are not observed, which is due to the large Van der Waals radius of bromine.

(vi) In addition, $(CaBr_2)_6$ has been investigated. It consists predominantly of two-fold edge sites, one three-fold coordinated face-site, and two corner sites (cf. Figure 3(f)). The spectral simulations of these species (not shown) indicate that the spectral shifts become quite similar to the bulk crystal (cf. Figure 4(l)).

(vii) Properties of the crystalline solid were simulated by $(CaBr_2)_{22}$, using the known geometry (a = 6.55 Å, b = 6.88 Å, c = 4.34 Å).[44] The structure of this solvated cluster is shown in Figure 3(g). The near-edge structure of the surface sites is quite similar to each other (cf. Figure 4(k)). It is similar to the bulk value (cf. Figure 4(l)), showing the largest red-shift as compared to the solvated anion.

(viii) For a comparison the structure of the crystalline calcium bromide hexahydrate $(CaBr_2 \cdot 6\ H_2O)$ is considered. Its structure is described by the space group P321, with lattice constants $a = b = 8.164$ Å, $c = 4.016$ Å, and an angle $\gamma = 120°$[27,44] (cf. Figures 3(h) and 4(f)). The computed near-edge spectrum is similar to the corner sites in clusters (see above). There is clearly a visible shoulder in the near-edge regime, which is evidently due to the Br^-–H_2O intermolecular bond, where the distance between Br^- and O is reported to be 3.36 Å.[28]

The building block approach of the core level spectra, which becomes evident due to spectral shifts of the near-edge features, is quantified by using reduced bromine anion binding energies *BE* in variable size aggregates relative to the fully solvated Br^- occurring in dilute solutions. This quantity is normalized to the binding energies of a Bjerrum pair $CaBr^+$ ($BE_{ion-pair}$), corresponding to the ratio $BE_{ion-clust}/BE_{ion-pair}$. These quantities are determined from the same formulas as used above for MD calculations:

$$BE = \sum_i \left[-\frac{q_{Br^-} q_i}{4\pi\varepsilon_0 r_i} + 4\varepsilon_i \left[\left(\frac{\sigma_i}{r_i}\right)^{12} - \left(\frac{\sigma_i}{r_i}\right)^{6} \right] \right]. \quad (3)$$

Here, q_{Br^-} is the charge of the central bromine ion; q_i and r_i are the charges and the distances to all ions in the variable size clusters, respectively; ϵ_i and σ_i are the Lennard-Jones parameters of Br^- interactions with the nearest neighbor Ca^{2+} ions given above for MD calculations. Note that Lennard-Jones interactions with distant ions are neglected. The calculated reduced bromine anion binding energy in clusters is plotted as a function of red-shift of the bromine K-edge, yielding a linear correlation, as shown in Figure 5. This plot indicates that distinct sites in clusters provide similar spectral shifts for small clusters $(CaBr_2)_n$, with $n \leq 6$, justifying the building block approach for small pre-nucleation clusters. For the solid the value for Br^- is estimated on the basis of the Madelung constant of the $CaCl_2$ crystal,[45,46] which is slowly approached as the cluster size increases. However, for small clusters each cluster size provides an intensity pattern in near-edge structure, which is due to the number density of the geometrical sites, providing a unique pattern that can be used to assign the experimental results. Thus, the experimental near-edge spectra are reconstructed by the weighted sum over all calcium bromide clusters $(CaBr_2)_i$ formed in supersaturated solution:

$$I_{total} = \sum_{clusters} c_i I_i. \quad (4)$$

Here, c_i is the fitted concentration of variable size clusters in solution and I_i corresponds to the spectral shape of each model structure described above, whereby

$$I_i = \sum_{sites} n_j I_j. \quad (5)$$

Here, n_j is the number of j-type sites in the cluster of the size i. The mixing ratio of clusters changes as a function of S, explaining the observed spectral shifts shown in Figure 2. This analysis provides the following results: The experimental spectrum recorded at S = 0.38 contains exclusively fully solvated Br^-, which is in full agreement with previous work.[28] There, EXAFS measurements supported by MD correlation functions, show a broad peak at $r_{Ca\text{-}Br} = 5.0$ Å indicating a hydration number of 6 for Ca^{2+}. This is typical for precursors of $CaBr_2 \cdot 6H_2O$.

At $S = 1$ the solvation shell of Br^- is broken and aggregation starts to occur. The evidence comes from an EXAFS analysis and MD correlation functions for concentrated $CaBr_2$ solutions (≈56%),[38] which is similar to the values deduced above from the experimental results (cf. Figure 2 and Table I). The Ca^{2+}–Br^- distance of 3.05 Å is fully reproduced by MD calculations performed in this work. Formation of such contact ion pairs in highly saturated solutions was also reported before.[47] Considering the formation of dimers the corner-to-edge ratio C/E should be 3. From the experimental results, which are used to adapt the structural building block model, one derives for $S = 1$ that the mixing ratio between the contact ion pair (Bjerrum pair $CaBr^+$), dimers, and solvated Br^- should be ≈7:5:4. This implies that the spectral shift of the core level absorption spectrum at S = 1 relative to S = 0.38 is essentially due to contributions from singly coordinated corner sites and doubly coordinated edge sites. Figure 6 shows the comparison of the experimental results

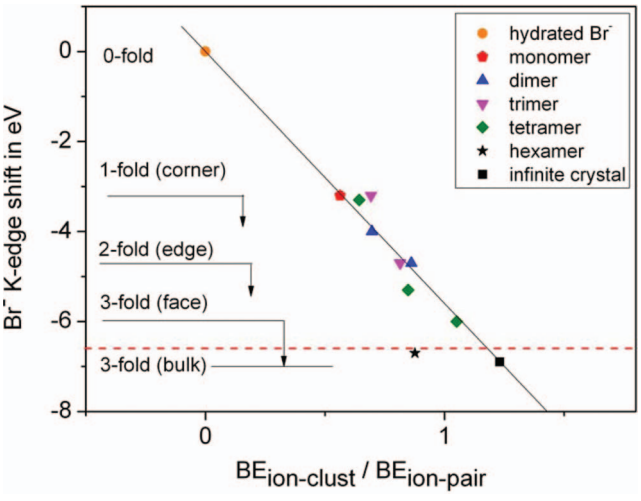

FIG. 5. Correlation of the calculated Br K-edge shift as a function of the reduced binding energy for different sites in variable size $CaBr_2$ pre-nucleation clusters $(CaBr_2)_n$. At $n \geq 6$ the shifts are similar to the bulk value of the crystal, so that the dashed line indicates the limit of the size sensitivity of core level spectra. Arrows indicate the calculated K-edge regimes relative to the solvated bromine anion for differently coordinated bromine sites (see text for further details).

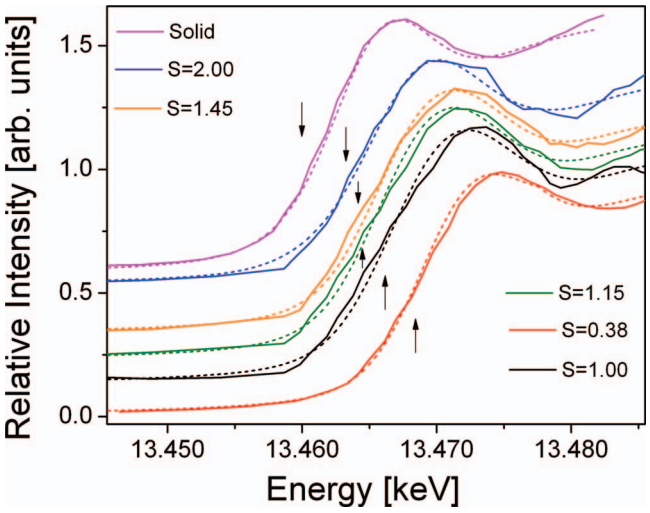

FIG. 6. Comparison of the experimental (full lines) and calculated (dashed lines) Br K-edges at different saturation ratios S of aqueous $CaBr_2$ solutions. Arrows indicate the position of the Br K-edge.

(full curves) and the simulated spectra (dashed curves) using the building block approach. Note, that for all simulations shown in Figure 6 an additional Gaussian broadening of the spectral features of 3.6 eV was added to the Voigt profiles in order to account for cluster solvation in the linear correlation shown in Figure 5. For S = 1.15 enhanced formation of dimers has to be taken into account. Keeping in mind the 3:1-ratio of two-fold coordinated edge sites, as compared to singly coordinated corner sites, one derives best agreement with the experimental results for a dimer-to-monomer ratio of 7:1. This clearly indicates that the cluster size increases with S and the composition of clusters can be plausibly rationalized. The near-edge spectrum at S = 1.45 is similar in shape as that of S = 1.15, corresponding to a dominating dimer mixing ratio. The simulation of the near-edge spectrum at $S = 2$ (cf. Figure 2) requires to consider threefold of coordinated face sites, which occur for clusters that are at least trimers. A mixture of tetramers $(CaBr_2)_4$ and trimers $(CaBr_2)_3$ provides for corner (C), edge (E), and face (F) sites a ratio of C:E:F = 5:1:1, yielding best resemblance to the experimental spectra at S = 2. Threefold coordinated bulk sites (see Figure 4(k)) can be excluded, since they are prevailing for large volume-to-surface ratios, which would be typical for clusters containing more than 50 moieties. Such large clusters are excluded, since these are expected to be beyond the critical cluster size for spontaneous growth. Their contribution is only used for modeling the near-edge spectra of the crystalline powder of anhydrous $CaBr_2$ (see Figure 6).

Alternatively, one might consider structures of pre-nucleation clusters, which involve hydrates, especially since calcium bromide is initially dissolved in water and it is known that stable hydrates are known to form crystals.[26,27] Consequently, one might expect that in supersaturated solutions such species should be present as pre-nucleation clusters, as well. Evidently, such species exist, but the experimental shifts in near-edge spectra and the calculated spectrum shown in Figure 4(f) are not fully in line with this assumption. The findings rather indicate that cluster formation leads to the occurrence of solvated variable size clusters containing no water. Clearly, the spectral shifts in near-edge spectra at S ≥ 1.45 indicate that pre-nucleation clusters containing water can be excluded to be the origin of these spectral shifts. This is rather unexpected for a crystal system that forms solid hydrates upon crystallization from aqueous solution. This deviation is rationalized in terms of crystal growth processes on nuclei that might have a different structure than the macroscopic crystal. Evidence for such behavior has been found in recent modeling work on clathrates.[48] There, it was shown that the crystallinity of the core reduces its critical size and crystalline solids can even grow on amorphous cores. This implies for the present work that $CaBr_2$ pre-nucleation clusters may induce heterogeneous nucleation leading to solid hydrates.

V. CONCLUSIONS

Element-selective excitation of single supersaturated $CaBr_2$-solution droplets prepared by optical levitation in a controlled ambient atmosphere allowed us to study element-selectively the local surroundings of bromine sites by near-edge spectroscopy. This approach gives us clear insights into the occurrence of pre-nucleation clusters in supersaturated solutions. The present results are accompanied by significant and systematic spectral shifts of all spectral features near the Br K-edge. These are due to the formation of pre-nucleation clusters in aqueous solution, as evidenced from model calculations simulating the Br-K-near-edge spectra. The spectral shifts are shown to be site-specific, allowing for a determination of the composition of different sites in clusters as a function of supersaturation. The present approach represents, in general, a unique way to experimentally probe structural motifs of pre-nucleation clusters, which determine the subsequent growth processes upon spontaneous nucleation. In the case of $CaBr_2$ it is concluded that solvated, variable size pre-nucleation clusters contain no water, so that the experimental results cannot be rationalized in terms of hydrate clusters $(CaBr_2 \cdot 6\ H_2O)_n$.

ACKNOWLEDGMENTS

Financial support by the Bundesministerium für Bildung und Forschung (BMBF) (Grant No. 05K07KEB) is gratefully acknowledged.

[1] D. Erdemir, A. Y. Lee, and A. S. Myerson, Acc. Chem. Res. **42**, 621 (2009).
[2] S. T. Martin, Chem. Rev. **100**, 3403 (2000).
[3] S. M. Iveson, J. D. Litster, K. Hapgood, and B. J. Ennis, Powder Technol. **117**, 3 (2001).
[4] S. D. Durbin and G. Feher, Ann. Rev. Phys. Chem. **47**, 171 (1996).
[5] H. R. Pruppacher and J. D. Klett, *Microphysics of Clouds and Precipitation* (Kluwer, Dordrecht, 1998).
[6] M. Volmer and A. Weber, Z. Phys. Chem. **119**, 277 (1925).
[7] J. Lothe and G. M. Pound, J. Chem. Phys. **36**, 2080 (1962).
[8] A. F. Izmailov, A. S. Myerson, and H. S. Na, Phys. Rev. E **52**, 3923 (1995).
[9] R. Mohan, O. Kaytancioglu, and A. S. Myerson, J. Cryst. Growth **217**, 393 (2000).
[10] D. Gebauer, A. Völkel, and H. Cölfen, Science **322**, 1819 (2008).
[11] D. Gebauer and H. Cölfen, Nano Today **6**, 564 (2011).
[12] N. Pienack and W. Bensch, Angew. Chem., Int. Ed. **50**, 2014 (2011).
[13] J. Y. Gal, J. C. Bollinger, H. Tolosa, and N. Gache, Talanta **43**, 1497 (1996).
[14] R. Demichelis, P. Raiteri, J. D. Gale, D. Quigley, and D. Gebauer, Nature Commun. **2**, 590 (2011).
[15] V. Zelenay, M. Ammann, A. Krepelova, M. Birrer, G. Tzvetkov, M. G. C. Vernooij, J. Raabe, and T. Huthwelker, J. Aerosol Sci. **42**, 38 (2011).
[16] I. N. Tang and H. R. Munkelwitz, Atmos. Environ. **27**, 467 (1993).
[17] B. Steiner, B. Berge, R. Gausmann, J. Rohmann, and E. Rühl, Appl. Opt. **38**, 1523 (1999).
[18] B. Berge, K. Sudholz, B. Steiner, J. Rohmann, and E. Rühl, Phys. Chem. Chem. Phys. **1**, 5485 (1999).
[19] M. A. Hamza, B. Berge, W. Mikosch, and E. Rühl, Phys. Chem. Chem. Phys. **6**, 3484 (2004).
[20] S. E. Wolf, J. Leiterer, M. Kappl, F. Emmerling, and W. Tremel, J. Am. Chem. Soc. **130**, 12342 (2008).
[21] M. Grimm, B. Langer, S. Schlemmer, T. Lischke, U. Becker, W. Widdra, D. Gerlich, R. Flesch, and E. Rühl, Phys. Rev. Lett. **96**, 066801 (2006).
[22] D. Duft, T. Achtzehn, R. Müller, B. A. Huber, and T. Leisner, Nature (London) **421**, 128 (2003).
[23] A. Ashkin, Phys. Rev. Lett. **24**, 156 (1970).
[24] C. Mund and R. Zellner, Chem. Phys. Chem. **4**, 630 (2003).
[25] B. J. Kennedy and C. J. Howard, Phys. Rev. B **70**, 144102 (2004).
[26] E. H. E. Pietsch, *Gmelins Handbuch der Anorganischen Chemie* (VCH, Weinheim, 1957).
[27] A. Leclaire and M. M. Borel, Acta Crystallogr., Sect. B **33**, 2938 (1977).
[28] F. Jalilehvand, D. Spangberg, P. Lindqvist-Reis, K. Hermansson, I. Persson, and M. Sandström, J. Am. Chem. Soc. **123**, 431 (2001).
[29] J. L. Fulton, S. M. Heald, Y. S. Badyal, and J. M. Simonson, J. Phys. Chem. A **107**, 4688 (2003).

[30]A. M. Gaspar, M. A. Marques, M. I. Cabaco, M. I. D. Marques, T. Buslaps, and V. Honkimaki, J. Mol. Liq. **110**, 15 (2004).
[31]A. Erko, I. Packe, C. Hellwig, M. Fieber-Erdmann, O. Pawlitzki, M. Veldkamp, and W. Gudat, AIP Conf. Proc. **521**, 415 (2000).
[32]P. D'Angelo, A. Di Cicco, A. Filliponi, and N. V. Pavel, Phys. Rev. A **47**, 2055 (1993).
[33]R. Flesch, A. A. Pavlychev, J. J. Neville, J. Blumberg, M. Kuhlmann, W. Tappe, F. Senf, O. Schwarzkopf, A. P. Hitchcock, and E. Rühl, Phys. Rev. Lett. **86**, 3767 (2001).
[34]K. Schaschek, J. Popp, and W. Kiefer, Ber. Bunsenges. Phys. Chem. **97**, 1007 (1993).
[35]K. Schaschek, J. Popp, and W. Kiefer, J. Raman Spectrosc. **24**, 69 (1993).
[36]G. Lippert, J. Hutter, and M. Parrinello, Mol. Phys. **92**, 477 (1997).
[37]Y. Joly, Phys. Rev. B **63**, 125120 (2001).
[38]H. Daiguji and E. Hihara, Heat Mass Transfer **35**, 213 (1999).
[39]A. L. Ankudinov, B. Ravel, and J. J. Rehr, Phys. Rev. B **58**, 7565 (1998).
[40]W. H. E. Schwarz, Chem. Phys. **11**, 217 (1975).
[41]Y. Joly, *FDMNES User's Guide* (Institut Néel, Grenoble, 2011), p. 45.
[42]S. I. Zabinsky, J. J. Rehr, A. Ankudinov, R. C. Albers, and M. J. Eller, Phys. Rev. B **52**, 2995 (1995).
[43]J. J. Rehr, A. Ankudinov, and S. I. Zabinsky, Catal. Today **39**, 263 (1998).
[44]R. W. G. Wykhoff, *Crystal Structures* (Interscience, New York, 1963).
[45]D. J. Green, *Introdcution to the Mechanical Properties in Ceramics* (Cambridge University Press, Cambridge, 1998).
[46]L. Glasser, Inorg. Chem. **51**, 2420 (2012).
[47]T. Yamaguchi, S. Hayashi, and H. Ohtaki, Inorg. Chem. **28**, 2434 (1989).
[48]L. Jacobson and V. Molinero, J. Am. Chem. Soc. **133**, 6458 (2011).